Pressure dependence of ZnDTP tribochemical film formation

A combinatorial approach

Originally published in:
Tribology Letters 28(2), https://doi.org/10.1007/s11249-007-9267-0

Tribol Lett (2007) 28:209–222
DOI 10.1007/s11249-007-9267-0

ORIGINAL PAPER

Pressure Dependence of ZnDTP Tribochemical Film Formation: A Combinatorial Approach

Roman Heuberger · Antonella Rossi · Nicholas D. Spencer

Received: 1 July 2007 / Accepted: 24 August 2007 / Published online: 15 September 2007

Abstract Combinatorial testing has been performed on zinc dialkyldithiophosphate (ZnDTP)-containing lubricants, to investigate the effects of contact pressure on the formation of tribochemical films. Contact pressures ranging from 25 to 500 MPa were applied in ball-on-disc tribotests with oscillating load. Both the ball and the disc were investigated by means of small-area and imaging X-ray photoelectron spectroscopy (XPS). The thickness and the composition of the reaction layer were estimated from the XPS data. The thickness of the reaction layer in the tribologically stressed areas of the ball and of the disc increased with both temperature and contact pressure. The reaction layer mainly consisted of short-chain poly(thio)phosphates, shorter chains being observed at higher contact pressures. At high pressures, the presence of a thick, high-toughness short-chain poly(thio)phosphate layer can explain the lower friction and dimensional wear coefficients observed. On the ball, similar anti-wear film formation mechanisms were observed as on the disc, zinc sulphide being deposited in the post-contact region.

Keywords X-ray photoelectron spectroscopy · XPS · ZnDTP · Boundary lubrication · Tribochemistry · Combinatorial testing · Load · Temperature · Friction · Wear

R. Heuberger · A. Rossi · N. D. Spencer (✉)
Laboratory for Surface Science and Technology, Department of Materials, ETH Zurich, Wolfgang-Pauli-Strasse 10, 8093 Zurich, Switzerland
e-mail: spencer@mat.ethz.ch

A. Rossi
Dipartimento di Chimica Inorganica ed Analitica, Università degli Studi di Cagliari, Cittadella Universitaria di Monserrato, 09100 Cagliari, Italy

1 Introduction

Combinatorial testing is frequently used in the pharmaceutical industry for rapid parallel screening. In tribology, friction and wear strongly depend on various experimental parameters such as the material of the tribopairs, their surface roughness and geometry, the lubricant composition, and the test conditions, such as contact pressure, sliding speed and temperature [1–3]. The investigation of the effect of all these parameters is both time consuming and laborious: the design of an experiment where a set of spatially separated areas are tested under different conditions, i.e. the development of a combinatorial approach to tribometry, allows high throughput in lubricant-additive testing. An example of a combinatorial test in tribology is the scratch test, where a diamond tip is slid over the surface with increasing load [4]. Hogmark et al. developed a crossed-sample configuration with load varying along the sample [4, 5]. Both tests have been used to screen load effects on hard coatings [4]. Eglin et al. developed two combinatorial approaches to ball-on-disc testing using a tribometer that allows the free programming of load, radius and rotational speed [6–9]. In the first approach, the effect of different loads were studied at different radii on a single disc [6–8]. The contact region was artificially expanded with closely spaced multiple radii to enable subsequent surface-analytical investigations of the tribotrack [7, 8]. In the second approach, the applied load was ramped up and down as a function of the geometrical position of the disc while different sliding times were applied at different radii; this approach focuses on the tribological results (friction, wear)

[9]. The application of different conditions at different radii seems to be a very effective and useful approach at low temperatures, while in some high-temperature experiments, the ongoing thermal reactions may influence the chemical composition of the tribofilm produced on another track created at an earlier stage of the experiment [10].

One of the aims of the present study was to set up a combinatorial test that could be effectively applied at both low and high temperatures without artificially expanding the contact region with closely spaced multiple radii. Earlier publications [7, 8, 11] relied on this approach in order to overcome the resolution limits of the XPS instruments employed. The newer generation of XPS spectrometers, however, is able to focus a monochromatic X-ray beam down to 5–10 μm, and this allows imaging and small-area XPS measurements to be performed on single wear tracks produced in a ball-on-disc experiment.

Zinc dialkyldithiophosphate (ZnDTP, formula is in Fig. 1)—a family of organometallic compounds—is still widely used as an anti-wear additive and exhibits excellent performance under boundary-lubrication conditions [12, 13]. The disadvantage of ZnDTPs is that they contain large amounts of phosphorus, sulphur and zinc, which impair the environment, both directly and indirectly, by poisoning exhaust catalysts. For this reason environmental legislation will be limiting the concentration of phosphorus and sulphur in engine oils: Replacements for ZnDTP, as well as an understanding of the working mechanisms of both ZnDTP and its possible alternatives, are badly needed.

Much effort has been expended in understanding the anti-wear mechanism of ZnDTP, especially its temperature dependence. Tribochemical films produced from ZnDTP have been investigated with numerous tools, such as atomic force microscopy (AFM) [14–17], nano-indentation [17–20], XPS [7, 11, 20–22], X-ray absorption spectroscopy (XANES) [22–24] and in situ attenuated total reflection infrared spectroscopy [25, 26]. The current understanding is that thermal degradation of ZnDTP begins with the migration of the carbon chain from the oxygen atom to the sulphur atom at temperatures as low as 60 °C [11, 27–29]. Some of the carbon chains and some thiols are released into the lubricant solution [11, 30]. Starting below 100 °C, phosphoryl groups react with each other to form a pyrophosphate $P_2O_7^{4-}$, also known as "short-chain polyphosphates". At higher temperatures (above ~150 °C), higher concentrations of fragments are available in the lubricant and the

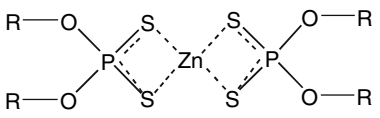

Fig. 1 Chemical formula of zinc dialkyldithiophosphate (ZnDTP)

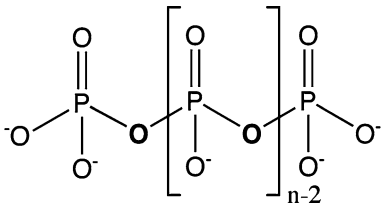

Fig. 2 Scheme of a polyphosphate with the chain length *n*. The oxygen atoms linking two phosphorus atoms together (*bold*) are denoted "bridging oxygen" (BO), while the terminal oxygen atoms in the phosphate groups are labelled "non-bridging oxygen" (NBO) [31]

formation of longer chains, known as polyphosphates (see Fig. 2), can occur [11–13, 24]. It has been suggested that during a tribological contact similar reactions occur on the surfaces of both counterparts, starting at room temperature [11, 32]. But while it has been proven that the tribofilm changes on the disc as a function of test temperature from a zinc phosphate at low temperature to a zinc polyphosphate at higher temperature [11, 20, 22, 25, 26] only very little analysis of the ball has been carried out [33, 34].

The influence of load on the tribofilm composition has been examined by only a few research groups to date. While Bird and Galvin found only small effects within the experimental uncertainties [21], Eglin et al. working at ambient temperature, observed the formation of orthophosphates at a load of 5 N [7, 8] and Yin et al. found higher formation rates and longer polyphosphate chains with higher loads at 80 °C [35]. Although much effort has been put into understanding the reaction mechanism, there remain many open questions concerning the reacting species, the film formation and its kinetics [12, 13].

In this study, a modified combinatorial approach has been applied for the first time to investigate the pressure dependence of the formation mechanism of tribofilms. Pressure was varied from 26 ± 5 to 515 ± 100 MPa on a single tribotrack. Temperatures of 30 °C, 80 °C and 150 °C were investigated, as they all typically occur under different conditions in an automobile engine.

2 Experimental

2.1 Tribological Testing

A CETR UMT-2 tribometer with temperature control (Center for Tribology, Campbell, CA, USA) was employed for the ball-on-disc test. The load cell could be moved up and down and the normal load was generated by a compressed spring. Both ball and disc (both hardened bearing steel 100Cr6, AISI 52100) were immersed in the lubricant oil. A 1 wt.% solution of a commercial secondary zinc dialkyldithiophosphate ZnDTP (C_3H_7 + C_6H_{13}, see Fig. 1, HiTEC®7169, Afton Chemical Corporation, Richmond,

VA, USA, purified by liquid chromatography) in poly-α-olefin (Durasyn 166, Tunap Industries GmbH. & Co., Mississauga, Canada) was used as a lubricant. Tests were performed at 30 °C, 80 °C and 150 °C (all ±3 °C) and each test was repeated at least three times. The relative humidity was between 20% and 60%. Prior to the actual oscillating-load test, a running-in of the ball applying a load of 10 N was performed for 1000 turns with a sliding speed of 0.005 m/s at a radius of 6.0 ± 0.2 mm in ZnDTP solution. The running-in of the ball yielded a measurable flat contact area that was used to determine the contact pressure by dividing the applied load by the measured apparent contact area.

During the oscillating-load test, the load was changed from 0.5 to 10 N over two cycles in each rotation (see scheme in Fig. 5). The sliding speed was 0.005 m/s and 1000 turns at a radius of 5.0 ± 0.2 mm were performed. Before further investigation, the samples were rinsed and ultrasonically cleaned in ethanol (p.a.) for 3 min.

The data were processed with Matlab 7.1 software (The MathWorks, Inc., Natick, MA, USA) to visualize the friction coefficient in colour plots and to determine the friction coefficients in dependence on the applied load (average of 2000 values/load).

2.2 Laser Profilometry

The topography of the discs was measured by means of laser profilometry (UBM, type UBC 14, UBM Messtechnik GmbH, Ettlingen, Germany), in order to determine the amount of wear. A Kr^{++}-laser beam (beam size 1 μm, wave length 407 and 413 nm) was dynamically focussed onto the sample and the z-value measured (accuracy ±10 nm) [36]. The sample table can be laterally moved and an area of 13×13 mm^2 was measured with a resolution of 120 points/mm. The data were stored in a z-value matrix.

The wear rate was calculated with Matlab Software (V6.5). Radial profiles were read out of the z-value matrix and averaged over sectors of 5° (50 lines) to improve the signal-to-noise ratio. Applying a linear background, the area below the background was summed and converted into wear rates.

2.3 X-Ray Photoelectron Spectroscopy

The surface chemistry of the tribostressed samples was investigated with X-ray photoelectron spectroscopy (XPS), analysing selected areas, both on the tribotrack and on the non-contact areas.

The X-ray source of the PHI Quantera SXM (ULVAC-PHI, Chanhassen, MN, USA) is a focussed and scanned monochromatic AlKα beam with a diameter that can be chosen between 5 and 200 μm. The emitted electrons are collected and retarded with an Omega lens system at an emission angle of 45°. After passing a spherical capacitor energy analyzer, the electrons are detected by a 32-channel detector. The system is equipped with a high-performance floating-column ion gun and an electron neutralizer for charge compensation. The residual pressure was always below 5×10^{-7} Pa. The system was calibrated according to ISO 15472:2001 and the accuracy was better than ±0.05 eV.

The unambiguous identification of the tribologically stressed areas was performed by means of the sample-positioning station (SPS), which allows photographs of the sample surface to be acquired outside the instrument. The SPS, in combination with a scanning X-ray image (SXI), facilitates rapid location of the desired analysis region and correlation with the coordinates calculated using the angular position from the tribological test. Two areas of the disc with each of the load values (10 N, 5 N and 0.5 N) were measured, as well as two non-contact areas. The arc length of the region tribostressed at any given load ±0.1 N was 165 μm and the width of the wear scar was ≤150 μm. On the ball, the centre of the tribostressed area, the non-contact areas 500 μm in front and behind the centre and, if present, the deposited material (approximately 250 μm behind the centre) were analysed. The positions of the points were double-checked with imaging XPS and XPS line scans.

Small-area XPS spectra were collected with a beam diameter of 20 μm and a power of 4.25 W in the constant-analyzer-energy (CAE) mode, using a pass energy of 69 eV and a step size of 0.125 eV. Under these conditions, the full width at half maximum height (fwhm) for $Ag3d_{5/2}$ is 1.3 eV. Survey spectra were acquired with 280 eV pass energy and a step size of 1 eV. The whole set of spectra (detailed and survey spectra) was acquired within 40–60 min/area. Imaging XPS and line scans were performed with a beam size of 10 μm, a power of 2.3 W and a pass energy of 140 eV in the snapshot mode, allowing the simultaneous acquisition of spectra with a binding-energy range of 15.5 eV. For imaging XPS, the spectra of all elements of interest were measured on an area of typically 600×600 μm^2 (lateral resolution normally 10 μm) within 6–8 h of acquisition.

2.3.1 Data Processing

Detailed spectra were processed with CasaXPS software (V2.3.12, Casa Software Ltd., UK). An iterated Shirley-Sherwood background subtraction was applied before peak fitting using a linear-least-squares algorithm. Minor charging was observed and corrected by referencing the aliphatic carbon to 285.0 eV. Details on the curve-fitting parameters, which have been measured on reference compounds, have been published elsewhere [10, 11].

2.3.2 Quantitative Analysis

Quantitative analysis was performed on the basis of a first-principles model [37, 38], assuming that the electrons from sublayers of a multilayer structure are attenuated by the overlayers according to the Beer-Lambert law. Further assumptions are that each layer is homogeneous in thickness and composition and that there are no gradients within the layers. The equations that correlate the area of the photoelectron signal with the concentration are written for each species of the substrate and for the multilayer structure according to [37, 38] and then solved numerically by iteration. Three-layer models based on these assumptions have been developed and applied by different groups to single- and multi-component substrates and overlayers [39–42] using a system of parametric equations.

In this work, since the substrate consists of only one component (i.e. iron), the system of equations can be simplified considerably, since the electrons from this single component are attenuated by the overlayer(s). Thus, in some cases, a film with four layers was proposed and the corresponding system of non-linear equations could still be solved using the Newton method. More details are provided in [10]. The presence of a four-layer structure—steel/oxide layer/reaction layer/organic layer—was proposed on the basis of angle-resolved profiles (not shown here). The peak areas were corrected with the sensitivity factor $S_i = \sigma_i \times L(\gamma) \times G(E_i) \times \rho/A_i \times \lambda(E_i) \times \cos(\theta)$, which includes the photoionization cross-section σ_i according to Scofield [43], the angular asymmetry function $L(\gamma)$ [44, 45], the étendue $G(E_i)$ as defined for Auger electron spectroscopy ($G(E_i) = \textit{analysed area} \times \textit{transmission function} \times \textit{detector efficiency}$) [37], the density of the material ρ divided by the atomic weight of the element A_i, the inelastic-mean-free path (IMFP) $\lambda(E_i)$ according to Tanuma et al. [46, 47] and $\cos(\theta)$, where θ is the emission angle. As model compounds for the densities of the layers and for calculating the IMFP, carbon, metallic iron, iron oxide Fe_3O_4, hydrated zinc orthophosphate for the reaction layer in the non-contact areas at 30 °C and 80 °C and zinc pyrophosphate for the tribofilms and the non-contact areas at 150 °C were chosen [11]. Details on the equations and factors mentioned above are given in [10].

3 Results

3.1 Tribological Tests

A colour plot of the friction coefficient μ of a typical tribological test performed at 80 °C is shown in Fig. 3. The load was cycled in such a way that the same angular position always experienced the same load. The friction coefficient changed only slightly during the first 500 turns and remained constant during the last 500 turns. Regions with lighter colour and therefore higher friction coefficient are to be found in the track at 0° (and 360°) and 180°, which correspond to the areas where the lowest load of 0.5 ± 0.1 N was applied. Slightly higher friction coefficients at lower loads were observed at all temperatures, as shown in Fig. 4. The friction coefficient increased with increasing temperature; for 10 N load it rose from 0.13 ± 0.01 at 30 °C to 0.15 ± 0.01 at 80 °C up to 0.20 ± 0.01 at 150 °C.

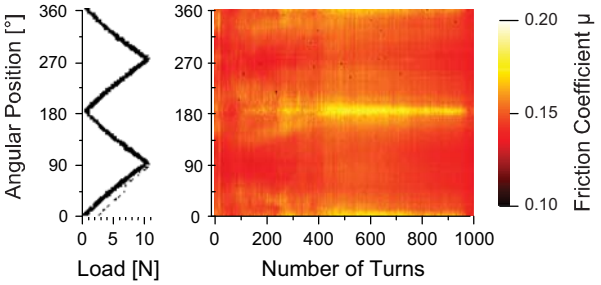

Fig. 3 Colour plot of the friction coefficient μ of a sample tribostressed at 80 °C in ZnDTP solution. Left: a plot of the applied load vs. the angular position of the rotating disc

3.2 Wear

The wear rate increased in a quasi-linear fashion with applied load (Fig. 5). High scatter of the wear rate due to the increased surface roughness caused by the wear was observed at high loads. The dimensional wear coefficients k (wear rates divided by the applied load, Fig. 6) showed lower average wear coefficients at higher loads. With increasing temperature, higher wear coefficients were obtained; for 10 N load, the wear coefficient increased from $1.1 \pm 0.6 \times 10^{-6}$ mm^3/Nm at 30 °C to $1.6 \pm 0.3 \times 10^{-6}$ mm^3/Nm at 80 °C to $1.8 \pm 0.7 \times 10^{-6}$ mm^3/Nm at 150 °C.

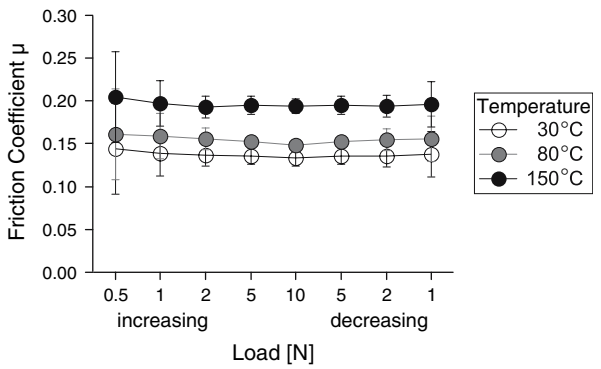

Fig. 4 Friction coefficient μ vs. load for experiments performed at different temperatures in ZnDTP solution

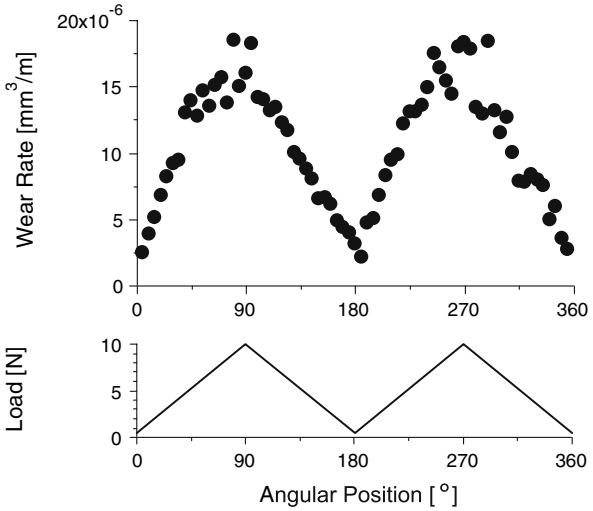

Fig. 5 Wear rate of a disc tribostressed at 80 °C in an oscillating-load test. The load dependence is shown as a function of the angular position of the disc in the scheme below

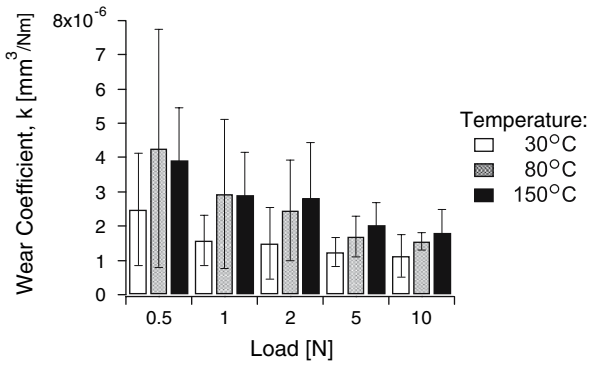

Fig. 6 Dimensional wear coefficient *k* on the disc as a function of the applied load for different temperatures of the ZnDTP solution

3.3 XPS Results

Survey and detailed high-resolution spectra were measured on both the disc and on the ball. Survey spectra were used for peak identification and to check the presence of contaminants. Detailed spectra of phosphorus 2p, together with zinc 3s, sulphur 2p, carbon 1s, oxygen 1s, iron 2p, zinc $2p_{3/2}$ and zinc LMM were recorded to identify the different chemical states of the species and to perform the quantitative analysis.

Spectra of a spot tribostressed with 10 N load at 80 °C are shown in Fig. 7. The *phosphorus 2p* signal was fitted with two peaks, $2p_{3/2}$ and $2p_{1/2}$, due to the spin-orbit splitting with an energy difference of 0.85 and an area ratio of 2:1. The phosphorus $2p_{3/2}$ peak was at 133.7 ± 0.1 eV. In the same spectrum the *zinc* 3s peak was at 140.5 ± 0.1 eV. This peak was used for the quantitative analysis instead of the more intense zinc $2p_{3/2}$ peak because the kinetic energy of the Zn3s electrons is closer to that of P2p and S2p and the IMFPs and therefore the sampling depths are similar.

The *sulphur* $2p_{3/2}$ peak was found at 162.2 ± 0.1 eV, and can be assigned to a sulphur having a formal oxidation state of –2, as found in sulphides [48, 49], thiolates [50, 51] or when sulphur is substituting oxygen atoms in poly(thio)phosphates.

In the *carbon 1s* spectrum, the most intense peak was at 285.0 eV due to aliphatic carbon [52, 53]. Minor contributions were found at 286.8 eV due to carbon bound to oxygen and sulphur [52, 54, 55] and at 289.0 ± 0.2 eV indicating carbonate [49, 56] and/or carboxylic groups [52, 55].

The *oxygen 1s* signal was composed of three peaks: the first at 530.3 ± 0.1 eV being assigned to oxygen in iron and zinc oxides [7, 57, 58], the main peak at 531.7 ± 0.1 eV to non-bridging oxygen (NBO) in polyphosphates and to oxygen bound to carbon [7, 59, 60] and the high-binding-energy peak at 533.4 eV to bridging oxygen (BO) in polyphosphates [60, 61].

The *iron* signal (Fig. 7) presented two main peaks at 711 and 724 eV due to the spin-orbit splitting, assigned to $Fe2p_{3/2}$ and $Fe2p_{1/2}$ [53]; only the more prominent iron $2p_{3/2}$ signal was used for quantification. On this sample, very low-intensity iron signals were detected. Peaks of two oxidation states Fe(II) and Fe(III) in iron oxides at 709.6 ± 0.1 and 711.0 ± 0.1 eV [49, 57, 58] were detected, while no signal attributable to metallic iron (707 eV) was revealed. Both oxides exhibit high-binding-energy satellites but only the satellite of iron (II) at 715.1 ± 0.1 eV was within the fitted region: it was fixed at an area of 7% of the main peak [57, 58]. A small, high-binding-energy peak at 713.5 eV assigned to iron phosphate [62] was detected.

3.3.1 Imaging XPS

Imaging XPS pictures and line scans were taken to determine the position of the analysed area and to check for lateral inhomogeneities of the tribotrack and of the non-contact area. The total peak area is colour coded and plotted as a function of the lateral position. In the case of oxygen, the spectra collected for the maps were additionally fitted with three peaks at 530.3, 531.9 and 533.4 eV and the maps reconstructed with a linear-least-square fit routine (see bottom row of Fig. 8).

Disc An example of the images collected on a tribotrack produced with 10 N at 80 °C and on the ball is shown in Fig. 8 to compare the films formed on both sliding partners. The tribotrack on the disc was clearly visible in the phosphorus 2p image, where the tribotrack showed higher

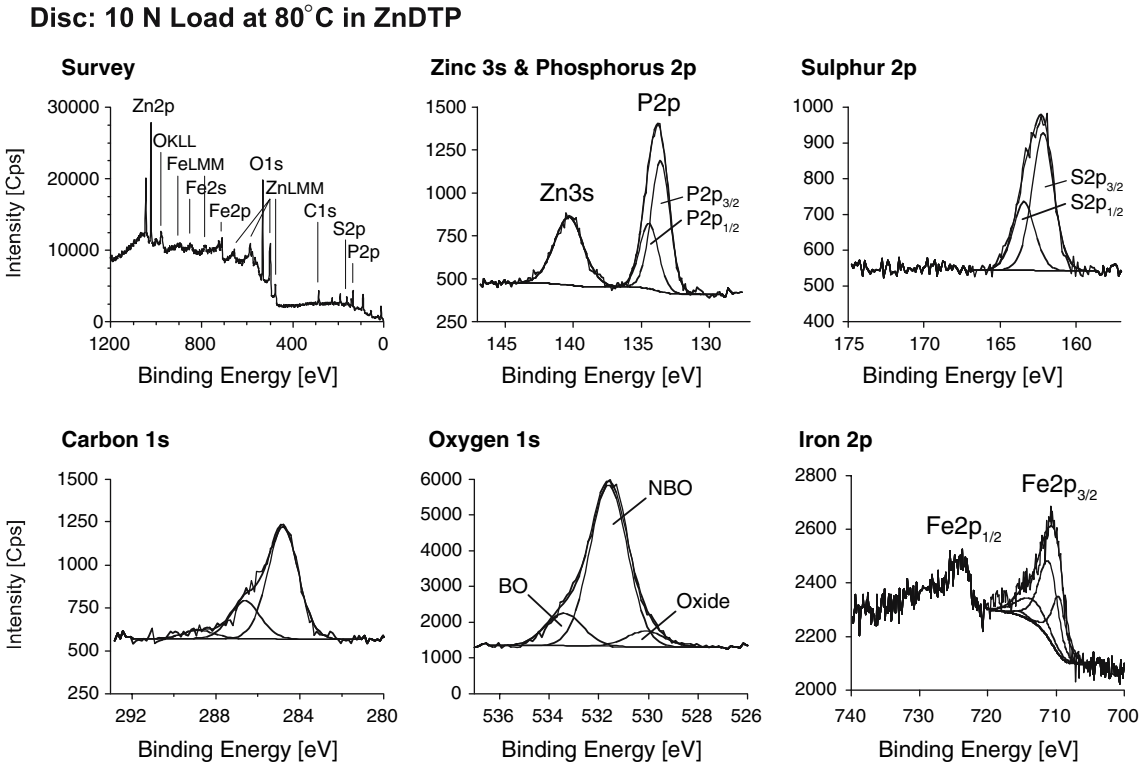

Fig. 7 XPS survey and detailed spectra of Zn3s and P2p, S2p, C1s, O1s and Fe2p measured on the tribotrack on the disc following an experiment under 10 N load at 80 °C. In the O1s spectrum the component at 531.8 eV is labelled as NBO, but this signal also contains contributions from sulphates and from oxygen bound to carbon

intensity than the non-contact area. The same distribution was found with the sulphur (II) peak at 162 eV binding energy. There was less contrast in the case of the peak at 168 eV, where slightly higher intensity was found in the non-contact area (not shown). To create the colour plots, the more intense zinc $2p_{3/2}$ peak was used instead of the Zn3s peak because of the better signal-to-noise ratio. Again the tribotrack shows a higher signal, and there was a region along the tribotrack with even higher intensity. The carbon image of the disc shows that there was slightly less carbon in the tribotrack than in the surrounding area, whereas the total oxygen map showed higher levels in the tribostressed region. The three different oxygen peaks showed that the oxide, which is more intense in the non-contact area, was covered with a film containing both non-bridging (NBO) and bridging oxygen (BO). The iron signal in the contact area appears lower than in the non-contact area due to the formation of a thicker reaction layer.

Ball In the tribostressed region on the ball (round area), the maps show higher intensities of the phosphorus, sulphur, zinc and NBO and BO signals; in this region, lower intensities of carbon, iron and O(oxide) signals were detected. In the region behind the contact area during the tribotest (left side of the contact area in the map), there was a tail with an enhanced intensity of both sulphur (II) and zinc.

3.3.2 *Spectra at Different Loads*

Disc Detailed spectra of P2p, Zn3s, S2p and O1s taken from small areas tribostressed with different loads, as well as from the non-contact area and of the centre of the ball are presented in Fig. 9. The spectra of areas tribostressed with 5 N were almost identical to those stressed with 10 N. A further decrease of the load to 0.5 N did not change the binding energy values of the photoelectron signals (uncertainty ±0.1 eV). The intensity of phosphorus, zinc and sulphur signals decreased with decreasing load, while the peak in the oxygen O1s spectrum assigned to the oxide became more pronounced.

In the *non-contact regions*, only low-intensity signals of phosphorus and zinc were detected at slightly lower binding energies of 133.4 ± 0.2 and 140.3 ± 0.1 eV. The sulphur peak at 162.1 ± 0.1 eV was much smaller compared to that measured in the 10 N area, but there was an additional noisy peak at 168.4 ± 0.3 eV that can be assigned to oxidized sulphur species [48, 49]. The non-contact region also revealed a more pronounced oxide peak at 530.0 ± 0.1 eV in the oxygen spectrum, while in the carbon spectrum, the high-binding energy peak (carbonates and/or carboxylic groups) at 288.8 ± 0.1 eV was more intense. The contributions to the O1s signals, labelled as

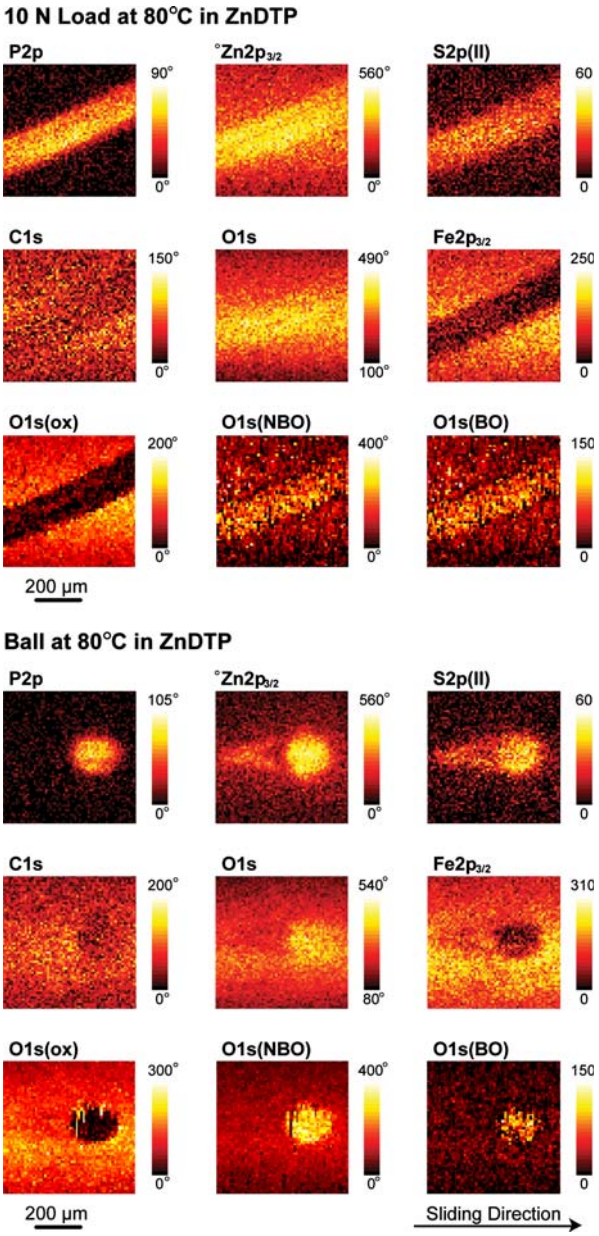

Fig. 8 Imaging-XPS of the tribotrack on the disc (tribostressed under 10 N load at 80 °C) and of the tribostressed region on the ball from the same experiment. Complete spectra were acquired at each point of the map and the area under the peak taken for the colour plot

NBO, also included those due to oxygen present in iron hydroxides and sulphate groups. In addition, adsorbed water has to be considered together with the BO-peak [58]. The iron peak in the non-contact region was very pronounced and metallic iron was detected at 706.7 eV. On some samples, small peaks at 711.8 eV assigned to iron hydroxide were found [7, 58].

Ball The peaks measured in the centre of the tribostressed region on the ball were similar to those collected on the disc after tribotesting with 5 and 10 N load, but a slightly higher intensity of the phosphorus and sulphur (II) peaks was observed.

3.3.3 Spectra at Different Temperatures

Disc Spectra of the 10 N area produced at 30 °C, 80 °C and 150 °C are presented in Fig. 10. At 30 °C, the binding energy of phosphorus $2p_{3/2}$ (133.6 ± 0.2 eV) was slightly lower than at 80 °C. A small sulphate peak was detected on the tribotrack and in the oxygen spectrum the peak of BO was less intense than that detected at 80 °C. The spectra from samples tribostressed at 150 °C were almost identical to those seen in the 10 N area produced at 80 °C; the binding energies of P2p, Zn3s and the low-binding energy peaks of S2p were each shifted by 0.2 eV, while the intensities of the peaks were similar. At this high temperature, minor contributions from sulphates were found in the tribotracks at 169.2 ± 0.1 eV. Almost no oxide peak in the oxygen signal and only weak iron signals were revealed. The spectra of the areas tribostressed with 0.5 N load showed intermediate characteristics between those of the high loads and the non-contact area.

The spectra of the non-contact areas at 30 °C were almost identical to those of the non-contact region of the 80 °C samples, while those recorded at 150 °C were similar to the tribostressed spectra, with slightly less intense phosphorus peaks but a higher intensity in the sulphate peaks. Only traces of iron were detected.

Ball On the tribostressed regions on the balls at all temperatures, similar spectra were observed as on the tribotracks on the discs stressed with high loads.

3.3.4 Thickness and Composition

Results of angle-resolved XPS profiles (not shown in this work) suggest that the surface was not uniform within the XPS sampling depth [10]. On the steel substrate an iron oxy-hydroxide layer was formed, covered by a reaction layer containing phosphorus, sulphur, zinc, iron phosphate and the two oxygen species NBO and BO. The outermost part of the surface presented an organic layer containing the contribution to the C1s signal due to aliphatic and high-binding energy carbons and some oxygen bound to carbon (contributing to the NBO peak). The same multilayer structure was found on similar samples in earlier work [9, 11]. The four-layer model was applied if the intensity of metallic iron was at least 5% of the overlayer intensity [63] and a three-layer model—assuming a semi-infinite oxide layer as a substrate—was used if this criterion was not met. Applying the multi-layer models, the thicknesses and compositions of the individual layers could be calculated simultaneously.

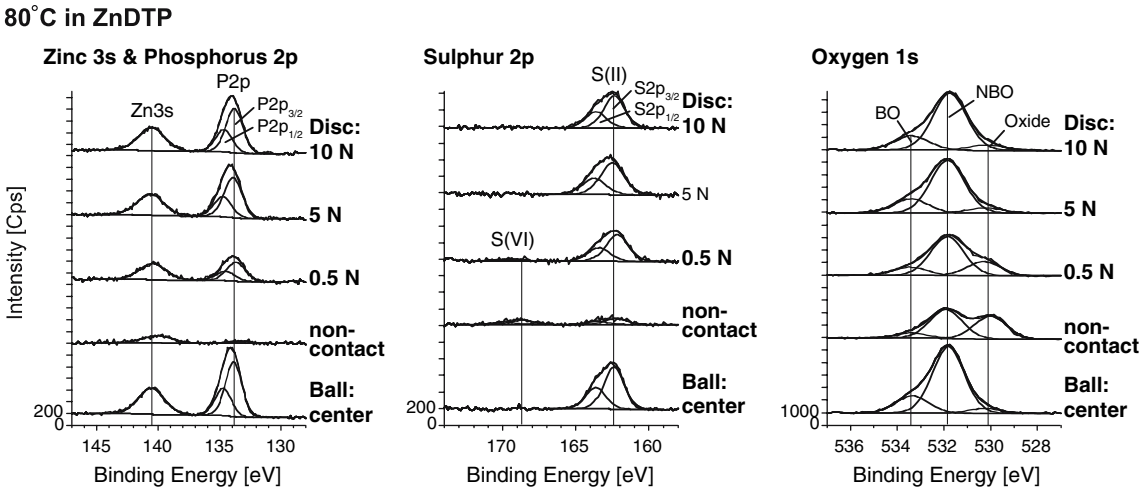

Fig. 9 XPS spectra of P2p with Zn3s, S2p and O1s measured in the tribotrack stressed under varying load, on the non-contact area on the disc and in the centre of the tribostressed region of the ball. The experiment was performed at 80 °C

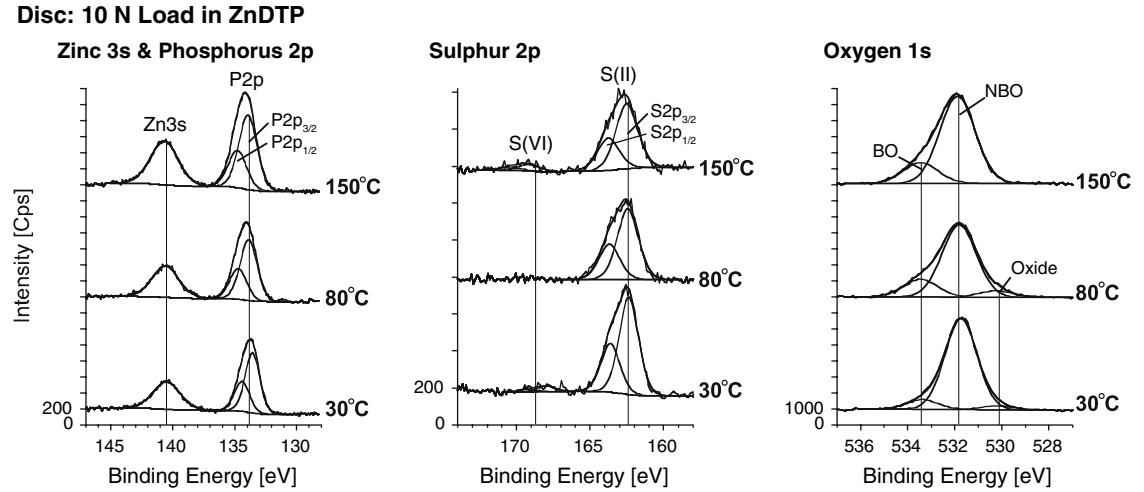

Fig. 10 XPS spectra of Zn3s and P2p, S2p and O1s measured in the tribotrack on the disc stressed with 10 N load at 30 °C, 80 °C and 150 °C

Thickness The thicknesses of the reaction layers are shown in Fig. 11 for different loads and temperatures. At both 30 °C and 80 °C, films of about 4 nm were formed at 5 N and 10 N loads, while in the non-contact areas of both the disc and the ball only very thin films of less than 1 nm were found. In the tribostressed region in the centre of the ball, similar thicknesses were measured as on the disc stressed at high loads. At 80 °C, the deposited material behind the contact region of the ball (compare with Fig. 8) led to an increased film thickness of 3.7 ± 0.4 nm compared to the non-contact areas of the same samples (1.4 ± 0.7 nm).

At 150 °C, tribofilms of 6 nm or thicker were formed on the disc. When the layers had a thickness higher than 6 nm no signal from the iron oxide layer was detected and the reaction layer has to be assumed to be semi-infinite and the thickness of the film is reported as being higher than 6 nm. Thinner films of 4 ± 1 nm were observed with 0.5 N load. In the non-contact areas, thick thermal films of more than 6 nm were produced. On the ball, thick reaction layers were found all over the surface.

Composition The composition of the reaction layer changed with the applied load and temperature (see Table 1). While on the tribotracks and the thermal films at 150 °C the amount of oxygen was about three times that of phosphorus, far more oxygen was present in the non-contact areas at 30 and 80 °C. Compared to the ZnDTP molecule, where a S:P ratio of 2:1 is present, a depletion of sulphur was found in the tribotracks and non-contact areas, while on the ball the deposited material behind the tribological contact at 80 °C was enriched in sulphur. Small amounts of oxidized sulphur species were found in the non-

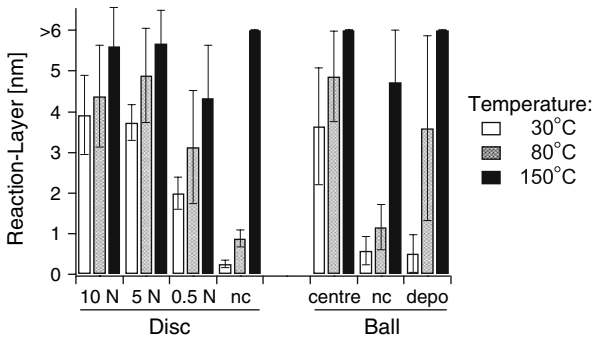

Fig. 11 Thickness of the reaction layer on the discs and balls as a function of the applied load and temperature. Please note that "nc" stands for the non-contact area, "centre" means the centre of the tribostressed region of the ball and "depo" is the deposited material on the ball. Reaction layers with thicknesses higher than 6 nm could not be calculated, therefore they are labelled as ">6"

contact areas only and in trace quantities in the tribotracks produced at 150 °C. In comparison to ZnDTP (Zn:P = 0.5:1), the reaction layers were enriched in zinc. Usually only small amounts of iron in the form of iron phosphate were to be found.

For the tribofilms at 30 °C, the oxygen-to-phosphorus ratio of 2.9 ± 0.1:1 is lower than expected for a short-chain polyphosphate. This might suggest that some sulphur (II) has most likely substituted oxygen in the phosphate chain. The tribofilm thus mainly consisted of a short-chain zinc poly(thio)phosphate, together with traces of zinc sulphide. At 30 °C, almost no changes in the film composition were observed with decreasing load. In the non-contact areas, there were small amounts of zinc oxide with traces of phosphate compounds and sulphides.

The 10 N tribofilm produced at 80 °C mainly contained short-chain zinc poly(thio)phosphate, with some sulphides. Applying a 5 N load led to the same film composition, and with 0.5 N there was slightly more sulphur present. The non-contact film was similar to that at 30 °C, but with higher amounts of zinc sulphide and zinc sulphate.

At 150 °C, the 10 N tribofilm was made of short-chain zinc poly(thio)phosphate, together with small amounts of zinc sulphate and sulphides. Again the same film composition was found at 5 N load. At the lowest load of 0.5 N, the main compound was still zinc poly(thio)phosphate, but the film contained more zinc sulphide and sulphate. Some iron substituting for zinc was detected as well. In the non-contact area there was a long-chain zinc poly(thio)phosphate with higher amounts of zinc sulphate and zinc sulphide.

The O/Fe ratio of the layer beneath the surface film was found to be equal to 1.3, in excellent agreement with the expected value, assuming the presence of an iron oxide (Fe_3O_4) layer on the steel surface [10]. This finding validates the model proposed here for the calculation of the

Table 1 Elemental ratio of the reaction layer normalised to phosphorus

			O	:	P	:	S(II)	:	S(VI)	:	Zn	:	Fe
30 °C	Disc	10 N	2.9 ± 0.1	:	1.0	:	0.5 ± 0.1	:	0.0	:	0.7 ± 0.1	:	0.1 ± 0.1
		5 N	2.8 ± 0.3	:	1.0	:	0.5 ± 0.1	:	0.0	:	0.7 ± 0.1	:	0.1 ± 0.0
		0.5 N	2.9 ± 0.5	:	1.0	:	0.5 ± 0.1	:	0.0	:	0.8 ± 0.1	:	0.0
		nc	8 ± 3	:	1.0	:	0.7 ± 0.7	:	0.4 ± 0.8	:	4.4 ± 1.8	:	0.0
	Ball	centre	2.8 ± 0.2	:	1.0	:	0.5 ± 0.1	:	0.0	:	0.6 ± 0.1	:	0.1 ± 0.0
		nc	6 ± 2	:	1.0	:	0.3 ± 0.1	:	1.0 ± 0.7	:	1.2 ± 0.5	:	0.0
80 °C	Disc	10 N	2.5 ± 0.3	:	1.0	:	0.5 ± 0.1	:	0.0	:	0.9 ± 0.1	:	0.0
		5 N	2.6 ± 0.2	:	1.0	:	0.5 ± 0.1	:	0.0	:	0.9 ± 0.1	:	0.0
		0.5 N	3.0 ± 0.4	:	1.0	:	0.7 ± 0.1	:	0.0	:	1.1 ± 0.1	:	0.0
		nc	10 ± 3	:	1.0	:	1.9 ± 0.5	:	1.0 ± 0.6	:	7 ± 2	:	0.0
	Ball	centre	2.8 ± 0.2	:	1.0	:	0.4 ± 0.0	:	0.0	:	0.7 ± 0.1	:	0.0
		nc	6 ± 3	:	1.0	:	1.4 ± 1.0	:	0.7 ± 0.8	:	2 ± 2	:	0.1 ± 0.1
		depo	4 ± 2	:	1.0	:	6 ± 1	:	0.6 ± 0.6	:	5 ± 2	:	0.0
150 °C	Disc	10 N	3.0 ± 0.2	:	1.0	:	0.3 ± 0.0	:	0.1 ± 0.1	:	0.9 ± 0.1	:	0.0
		5 N	2.9 ± 0.2	:	1.0	:	0.3 ± 0.1	:	0.0	:	0.9 ± 0.1	:	0.0
		0.5 N	3.3 ± 0.5	:	1.0	:	0.4 ± 0.1	:	0.1 ± 0.1	:	0.9 ± 0.1	:	0.1 ± 0.1
		nc	3.8 ± 0.2	:	1.0	:	0.9 ± 0.3	:	0.3 ± 0.1	:	1.5 ± 0.1	:	0.0
	Ball	centre	2.9 ± 0.0	:	1.0	:	0.3 ± 0.0	:	0.0	:	0.8 ± 0.0	:	0.0
		nc	4.3 ± 0.0	:	1.0	:	1.3 ± 0.1	:	0.4 ± 0.0	:	1.8 ± 0.1	:	0.0
		depo	3.4 ± 0.0	:	1.0	:	1.2 ± 0.0	:	0.3 ± 0.0	:	1.6 ± 0.0	:	0.0

In the case of oxygen, only the NBO and BO peaks were taken into account. For iron, only the peak assigned to iron phosphate was attributed to the reaction layer

composition and the thickness of the surface layers and of the substrate.

The composition of the tribofilm on the *ball* was very similar to that of tribofilms produced on the disc at high loads; no significant differences were detected. The non-contact areas on the ball half a millimetre in front of and behind the contact were equivalent, within the usual uncertainty, and similar to the non-contact areas on the disc. The material deposited at 80 °C about 250 μm behind the sliding contact mainly consisted of zinc sulphide. At 150 °C, the composition of the deposited material was similar to that of the non-contact areas.

3.3.5 *Chain Length*

The binding energy of phosphorus $2p_{3/2}$ can be used to identify the kind of phosphate formed on the surface: i.e. between orthophosphates (single phosphate groups), or short- or long-chain polyphosphates [7, 59, 60, 62, 64]. The chain length of these polyphosphates can be calculated using the BO-to-NBO ratio (see Fig. 12). The ratios were corrected by subtracting the contributions to the NBO signal of oxygen in sulphate groups and oxygen bound to carbon in the organic layer.

At both 30 °C and 80 °C, shorter chain lengths were observed corresponding to higher contact pressures. In the non-contact areas of 30 °C and 80 °C, the binding energy of phosphorus $P2p_{3/2}$ of 133.3 ± 0.2 eV indicates that orthophosphates were present [59]. The BO-to-NBO ratio of the non-contact areas is not plotted for these temperatures, because adsorbed water was contributing to the BO peak of these samples.

At 150 °C, chains of ~4 phosphate groups were found at high contact pressures while shorter chains of three units were found at low pressures. This was confirmed by the binding energy of phosphorus being at 134.0 ± 0.2 eV at high pressures and 0.2 eV lower at low pressure. In the non-contact areas, the thermal film consisted of a long-chain polyphosphate, as indicated by the BO-to-NBO ratio of almost 0.5.

The chain length of the tribostressed region on the *ball* remained unchanged with the applied temperature and ranged between 3 and 6 phosphate units. In the non-contact areas and in the near contact area (deposited material) at 150 °C, long chains were calculated.

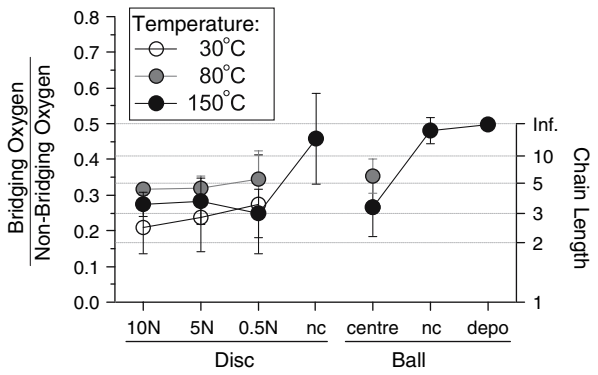

Fig. 12 Bridging to non-bridging oxygen ratio vs. the applied load and temperature. The ratio is corrected for the contributions to NBO originating from sulphate groups and carbon bound to oxygen

4 Discussion

4.1 Comparison of the Constant-Load and Oscillating-Load Approaches

In this paper, the modified combinatorial approach with oscillating load in combination with surface analysis using XPS is presented for the first time. The friction coefficients measured with the oscillating-load test (Fig. 4) are in excellent agreement with earlier work performed on the same system but with constant loads: applying the constant-load test, the friction coefficient increased from 0.14 ± 0.02 at room temperature to 0.20 ± 0.2 above 130 °C [11]. Only few data are to be found in the literature comparing the friction coefficient in a ZnDTP solution at different loads. For experiments with constant loads at 150 °C in ZnDTP solution, Eglin et al. [9] reported friction coefficients at 1 N and 5 N load of 0.19 ± 0.1, in agreement with this work. At low loads, 0.1 N, a higher value of 0.27 ± 0.3 was found.

The dimensional wear coefficients k obtained with the hardened steel samples stressed with the oscillating-load test were between 1 and 4×10^{-6} mm^3/Nm (see Fig. 6), which correspond to severe wear. This is unsurprising in the boundary-lubrication regime and the wear coefficients k would normally be expected to lie between 10^{-8} and 10^{-6} mm^3/Nm [1]. There are two reasons for the high wear rates observed in these experiments: First, the sliding speeds are very low and second, the contact areas are small, resulting in a high average contact pressure up to 500 MPa, even at relatively low applied loads.

The tribological films formed in this study were thicker than those formed in the constant-load test, while the thermal films had similar thicknesses [11]. This is likely to be due to the longer time of tribostress; only five turns per annulus were applied in the constant-load test, while 1000 turns were carried out with the oscillating-load test applied in this work. Short-chain poly(thio)phosphates with 2–6 phosphate units were found at all temperatures in the tribotracks, which corresponds to results obtained with constant loads [11, 65] and is in agreement with proposals made in the literature [22, 35]. At 150 °C, the thermal film

was composed of long-chain poly(thio)phosphates, in agreement with previous work [11, 29].

A potential drawback of the oscillating-load test approach is that part of the film formed at high contact pressure might be transferred to areas at low contact pressures [33, 34]. However, no evidence for a possible transfer was found and the results are in agreement with results obtained with the constant-load test [11].

4.2 Influence of Contact Pressure on Thickness and Composition of the Tribological Films

It is difficult to compare the applied loads reported in different studies, since often only the load is given but neither the contact pressure nor the contact area are reported. With applied loads ranging from 0.5 to 10 N in this work, average contact pressures in the range of 25–500 MPa were probed.

The tribological stress leads to the formation of poly(thio)phosphate tribofilms at all temperatures investigated, while in the non-contact areas only very thin thermal films were formed at 30 °C and 80°C. The contact pressure presumably leads to local frictional heating, which accelerates a chemical reaction of the adsorbed additives (see Fig. 13). Also, a purely tribochemical effect is likely: at 30 °C, iron phosphate was found in the reaction layer, which is an indication that nascent iron, released because of wear, reacts with the phosphoryl groups and forms a component of the tribofilm.

At 150 °C, thick thermal layers (>6 nm) composed of long-chain poly(thio)phosphates were formed. Under mechanical stress, there are further potential pathways: Wear might have removed the thermal layer, formed prior to contact, and upon tribostress a similar film-formation mechanism as at lower temperatures takes place [66]. Alternatively iron oxide reacts with the poly(thio)phosphates causing a shortening of the chains [67]. Iron is known to function as a depolymerising element for phosphate glasses [62]. Yet a further possibility is that the contact pressure leads to a cleavage of the long chains [11]. Any combination of these mechanisms could explain the presence of short-chain poly(thio)phosphates in the tribotracks.

At higher contact pressures, shorter poly(thio)phosphate chains were formed with correspondingly less sulphur. Only at 0.5 N load (150 °C) were shorter chains found than at higher contact pressures. An explanation might be that on the thick tribofilms formed under high contact pressure, only the outer part, which generally contains longer chains [22, 35, 65, 68], was probed, while at 0.5 N load the entire film, including the shorter chains at the bottom, were analysed. Less sulphur at higher contact pressures was also found by both Yin et al. and Eglin et al. [7, 8, 35], while Yin found longer chain lengths at higher contact pressures in an experiment at much higher sliding speed (0.35 m/s) at 100 °C [35], under which conditions a different lubrication regime may have been operative. According to nanoindentation measurements, the hardness of the tribofilm correlates with the applied contact pressure [17, 20]. Therefore a softer viscous film of longer chains might be present at lower contact pressures, which would explain the incrementally higher friction coefficient observed under these conditions. High contact pressures cause more frictional heating, therefore thicker films were formed in these areas. Together with the increased hardness at higher contact pressures, thicker and tougher films [69] of shorter polyphosphates were formed, which exhibited higher shear resistance, resulting in lower dimensional wear coefficients (see Fig. 6).

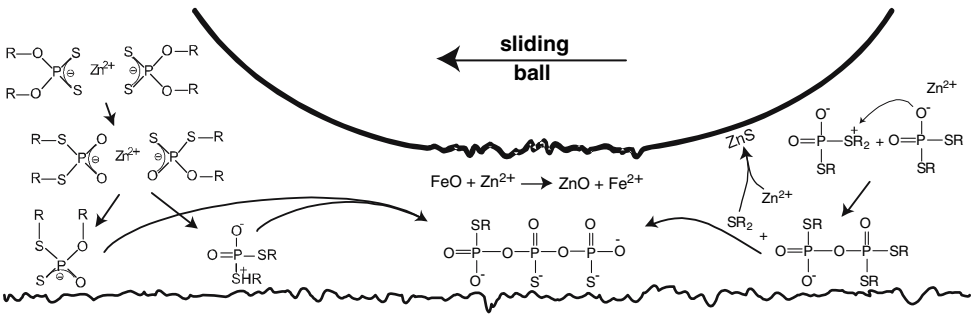

Off-contact Area:
- Below 100 °C: Adsorption of ZnDTP and reaction products.
- Above 130 °C: Thermal film formation.

Contact Area:
- Tribostress leads to partial removal of tribofilm with wear.
- Friction heat and shear stress leads to the formation of tribofilms with the adsorbed molecules.
- Transfer film to ball.

Near-contact Area:
- Friction heat leads to thermal decomposition and phosphate film formation.
- 80 °C: Alkylated sulphur reacts with Zn to ZnS, which is deposited.

Fig. 13 Schematic of reactions occurring in the contact, near-contact and off-contact areas on samples tribostressed under ZnDTP solution

4.3 Influence of Temperature on Thickness and Composition of Thermal and Tribological Films

In the non-contact areas at 30 °C and 80 °C, only very thin reaction layers of zinc sulphide and zinc phosphate were formed, whereas the films at 80 °C were thicker. This is in agreement with earlier temperature-dependent studies [11] and according to Bovington and Dacre, the thermal decomposition starts at 60 °C in the presence of iron powder as a catalyst [67]. At 150 °C, thick thermal films made of long-chain poly(thio)phosphate were formed, due to thermo-oxidative processes [3, 11, 29, 70]. The thickness and the P/S ratio measured on the thermal film formed in this investigation, after approximately 4 h of exposure to the ZnDTP-containing solution, were found to be 6 nm and 0.8 respectively: these values correlate well with those estimated on the basis of PIXE measurements (11 nm and with a P/S ratio of 1.5) after 8 h of exposure assuming the film to be composed of $Zn_2P_2O_7$ [24]. XPS thus allows the thickness and the composition of each layer, and simultaneously the composition of the substrate, to be calculated with very high flexibility and accuracy, since it is possible to use the proper density value for each layer.

In the tribostressed areas, the average thickness of the reaction layer increased with higher temperatures because of the external temperature, which together with the frictional heat favours the polyphosphate film formation. On the tribofilms formed at 150 °C, a reduced sulphide content was found while species containing oxidized sulphur were present. This is likely due to a temperature-dependent oxidation of the tribofilm [3].

4.4 ZnDTP Reactivity: Ball vs. Disc Surface Composition and Thickness

During a ball-on-disc experiment, the ball is under permanent tribostress while a single spot in the centre of the tribotrack is stressed for about 40 ms every 6.3 s. Despite the different rubbing time at varying loads experienced by the ball and the disc, both the thickness and the compositions of the reaction layers were the same for the tribostressed region on the ball and for the tribotrack on the disc stressed with high contact pressures (see Figs. 9 and 11 and Table 1): a short-chain poly(thio)phosphate of 2–6 units was always found with the same amount of sulphur (II) and zinc.

The non-contact areas on the ball 0.5 mm in front and behind the tribostressed region were essentially similar in thickness and composition as the non-contact areas on the disc, thus indicating that the thermal film was not affected because of the tribological contact half a millimetre away.

On the ball tribostressed at 80 °C, there was a tail behind the tribostressed region composed mainly of zinc sulphides (see Fig. 8 and Table 1). Upon frictional heating, reactive sulphur compounds are probably produced, which then react with zinc to form zinc sulphide and deposit behind the tribological contact. These products are readily detectable on the ball because they are always collected on the same area during the entire experiment, while on the other hand they are thinly distributed over the entire disc. At 30 °C no deposited material was found on the ball and at 150 °C, a thicker deposit behind the tribological contact than in the non-contact area was formed, with the same composition as that of the non-contact film. Thus at 150 °C, more reactive species were present in the vicinity of the tribological contact, leading to the thicker film.

5 Conclusion

Real applications, as opposed to most tribological tests, are characterised by long lifetimes with many stress cycles, often at different loads. This modified combinatorial approach now allows the screening of the effect of different loads along a single track, while the permanent change of the load does not appear to affect the frictional behaviour, as discussed above. This approach is far faster than changing the radius for each load and provides the possibility of performing long-term combinatorial experiments, which allow for a better comparison with real systems.

X-ray photoelectron spectroscopic characterization permitted not only the assessment of contact-pressure effects on the chemical composition, but also the calculation of thicknesses and compositions of the films formed both on the ball and on the disc. These findings help to understand the anti-wear mechanism of ZnDTP and allow the proposal of a mechanism that takes into account the changes occurring on the two counterparts. The same composition of the tribofilm was found on the ball and on the disc whenever high loads were applied. This suggests that the same mechanism took place on the ball and on the disc tribostressed with high contact pressures. While on the disc the pressure dependence was investigated, the reactions behind the tribological contact could be followed on the ball.

A higher contact pressure produced more frictional heat, which causes the formation of thicker tribofilms of poly(thio)phosphates. The higher pressure has the net effect of reducing the chain length, resulting in poly(thio)phosphates of 3–5 phosphate units. These films are presumed to be harder and tougher, which results in lower wear.

References

1. Hutchings, I.M.: Tribology – Friction and Wear of Engineering Materials. Butterworth-Heinemann Ltd, London (1992)
2. Hähner, G., Spencer, N.D.: Rubbing and scrubbing. Phys. Today **51**, 22–27 (1998)
3. Gellman, A.J., Spencer, N.D.: Surface chemistry in tribology. Proc. Inst. Mech. Eng. J. **216**, 443–461 (2002)
4. Hogmark, S., Jacobson, S., Larsson, M.: Design and evaluation of tribological coatings. Wear **246**, 20–33 (2000)
5. Hogmark, S., Jacobson, S., Waenstrand, O.: Universal test for friction, wear and lubrication, used in tribological studies. Swedish Patent, SE9802017-5 (1998)
6. Eglin, M., Rossi, A., Spencer, N.D.: Additive-surface interaction in boundary lubrication: a combinatorial approach. In: Proc. 28th Leeds-Lyon Symp., Vienna, pp. 49–57. Elsevier Science B.V. (2001)
7. Eglin, M., Rossi, A., Spencer, N.D.: X-ray photoelectron spectroscopy analysis of tribostressed samples in the presence of ZnDTP: a combinatorial approach. Tribol. Lett. **15**, 199–209 (2003)
8. Eglin, M., Rossi, A., Spencer, N.D.: A combinatorial approach to elucidating tribochemical mechanisms. Tribol. Lett. **15**, 193–198 (2003)
9. Eglin, M.: Development of a combinatorial approach to lubricant additive characterization. Ph.D. Thesis, ETH Zurich, Zurich, Switzerland (2003)
10. Heuberger, R.: Combinatorial study of the tribochemistry of antiwear lubricant additives. Ph.D. Thesis No. 17207, ETH Zurich (2007)
11. Heuberger, R., Rossi, A., Spencer, N.D.: XPS study of the influence of temperature on ZnDTP tribofilm composition. Tribol. Lett. **25**, 185–196 (2007)
12. Spikes, H.: The history and mechanisms of ZDDP. Tribol. Lett. **17**, 469–489 (2004)
13. Nicholls, M.A., Do, T., Norton, P.R., Kasrai, M., Bancroft, G.M.: Review of the lubrication of metallic surfaces by zinc dialkyldithiophosphates. Tribol. Int. **38**, 15–39 (2005)
14. Pidduck, A.J., Smith, G.C.: Scanning probe microscopy of automotive anti-wear films. Wear **212**, 254–264 (1997)
15. Aktary, M., McDermott, M.T., Torkelson, J.: Morphological evolution of films formed from thermooxidative decomposition of ZDDP. Wear **247**, 172–179 (2001)
16. Morina, A., Green, J.H., Neville, A., Priest, M.: Surface and tribological characteristics of tribofilms formed in the boundary lubrication regime with application to internal combustion engines. Tribol. Lett. **15**, 443–452 (2003)
17. Graham, J.F., McCague, C., Norton, P.R.: Topography and nanomechanical properties of tribochemical films derived from zinc dialkyl and diaryl dithiophosphates. Tribol. Lett. **6**, 149–157 (1999)
18. Bec, S., Tonck, A., Georges, J.M., Georges, E., Loubet, J.L.: Improvements in the indentation method with a surface force apparatus. Philos. Mag. A **74**, 1061–1072 (1996)
19. Warren, O.L., Graham, J.F., Norton, P.R., Houston, J.E., Michalske, T.A.: Nanomechanical properties of films derived from zinc dialkyldithiophosphate. Tribol. Lett. **4**, 189–198 (1998)
20. Bec, S., Tonck, A., Georges, J.M., Coy, R.C., Bell, J.C., Roper, G.W.: Relationship between mechanical properties and structures of zinc dithiophosphate anti-wear films. Proc. R. Soc. London A **455**, 4181–4203 (1999)
21. Bird, R.J., Galvin, G.D.: Application of photoelectron-spectroscopy to the study of e.p. films on lubricated surfaces. Wear **37**, 143–167 (1976)
22. Martin, J.M., Grossiord, C., Le Mogne, T., Bec, S., Tonck, A.: The two-layer structure of zndtp tribofilms Part 1: AES, XPS and XANES analyses. Tribol. Int. **34**, 523–530 (2001)
23. Yin, Z.F., Kasrai, M., Bancroft, G.M., Laycock, K.F., Tan, K.H.: Chemical characterization of antiwear films generated on steel by zinc dialkyl dithiophosphate using X-ray-absorption spectroscopy. Tribol. Int. **26**, 383–388 (1993)
24. Fuller, M.L.S., Fernandez, L.R., Massoumi, G.R., Lennard, W.N., Kasrai, M., Bancroft, G.M.: The use of X-ray absorption spectroscopy for monitoring the thickness of antiwear films from ZDDP. Tribol. Lett. **8**, 187–192 (2000)
25. Piras, F.M., Rossi, A., Spencer, N.D.: In situ Attenuated Total Reflection (ATR) spectroscopic analysis of tribological phenomena. In: Proc. 28th Leeds-Lyon Symp., Vienna, pp. 199–207. Elsevier Science B.V. (2001)
26. Piras, F.M., Rossi, A., Spencer, N.D.: Growth of tribological films: In situ characterization based on attenuated total reflection infrared spectroscopy. Langmuir **18**, 6606–6613 (2002)
27. Coy, R.C., Jones, R.B.: The thermal-degradation and ep performance of zinc dialkyldithiophosphate additives in white oil. ASLE Trans. **24**, 77–90 (1981)
28. Jones, R.B., Coy, R.C.: The chemistry of the thermal-degradation of zinc dialkyldithiophosphate additives. ASLE Trans. **24**, 91–97 (1981)
29. Fuller, M.L.S., Kasrai, M., Bancroft, G.M., Fyfe, K., Tan, K.H.: Solution decomposition of zinc dialkyl dithiophosphate and its effect on antiwear and thermal film formation studied by X-ray absorption spectroscopy. Tribol. Int. **31**, 627–644 (1998)
30. Luther, H., Sinha, S.K.: Zur Reaktionskinetik der thermischen Zersetzung von Zinkdialkyldithiophosphaten. Erdoel Kohle, Erdgas Petrochem. **17**, 91–97 (1964)
31. Brow, R.K.: Review: the structure of simple phosphate glasses. J. Non-Cryst. Solids **263**, 1–28 (2000)
32. Fujita, H., Spikes, H.A.: The formation of zinc dithiophosphate antiwear films. Proc. Inst. Mech. Eng. J. **218**, 265–277 (2004)
33. Minfray, C., Le Mogne, T., Lubrecht, A.A., Martin, J.M.: Experimental simulation of chemical reactions between ZDDP tribofilms and steel surfaces during friction processes. Tribol. Lett. **21**, 67–78 (2006)
34. Martin, J.M., Grossiord, C., Le Mogne, T., Igarashi, J.: Transfer films and friction under boundary lubrication. Wear **245**, 107–115 (2000)
35. Yin, Z.F., Kasrai, M., Fuller, M., Bancroft, G.M., Fyfe, K., Tan, K.H.: Application of soft X-ray absorption spectroscopy in chemical characterization of antiwear films generated by ZDDP.1. The effects of physical parameters. Wear **202**, 172–191 (1997)
36. Windecker, R.: Optical autofocussing profilometer. Techn. Messen. **60**, 267–270 (1993)
37. Seah, M.P.: Quantification of AES and XPS. In: Briggs, D., Seah, M.P. (eds.) Practical Surface Analysis, pp. 201–255. John Wiley & Sons Ltd, Chichester, UK (1990)
38. Fadley, C.S.: Solid state – and surface – analysis by means of angular-dependent x-ray photoelectron spectroscopy. Prog. Solid State Chem. **11**, 265–343 (1976)
39. Asami, K., Hashimoto, K.: X-Ray photoelectron-spectra of several oxides of iron and chromium. Corr. Sci. **17**, 559–570 (1977)
40. Rossi, A., Elsener, B.: XPS analysis of passive films on the amorphous alloy Fe70Cr10P13C7 – effect of the applied potential. Surf. Interface Anal. **18**, 499–504 (1992)
41. Elsener, B., DeFilippo, D., Rossi, A.: Composition of passive films on stainless steels formed in neutral sulphate solutions. In: Marcus, P., Baroux, B., Keddam, M (eds.) Modification of Passive Films, pp. 6–11. The Institute of Materials, London (1994)
42. Matsumoto, K.: Surface chemical and tribological investigations of phosphorus-containing lubricant additives. Ph.D. Thesis, ETH Zurich, Zurich, Switzerland (2003)
43. Scofield, J.H.: Hartree-Slater subshell photoionization cross-sections at 1254 and 1487 eV. J. Electron. Spectrosc. **8**, 129–137 (1976)

44. Reilman, R.F., Msezane, A., Manson, S.T.: Relative intensities in photoelectron-spectroscopy of atoms and molecules. J. Electron. Spectrosc. **8**, 389–394 (1976)
45. Seah, M.P.: Quantification of AES and XPS. In: Briggs, D., Grant, J.T. (eds.) Surface Analysis by Auger and X-Ray Photoelectron Spectroscopy, pp. 345–375. IM Publications and Surface Spectra Limited, Chichester and Manchester, UK (2003)
46. Tanuma, S., Powell, C.J., Penn, D.R.: Calculations of electron inelastic mean free paths. 5. Data for 14 organic-compounds over the 50-2000 eV range. Surf. Interface Anal. **21**, 165–176 (1993)
47. Tanuma, S., Powell, C.J., Penn, D.R.: Calculation of electron inelastic mean free paths (IMFPs) VII. Reliability of the TPP-2M IMFP predictive equation. Surf. Interface Anal. **35**, 268–275 (2003)
48. de Donato, P., Mustin, C., Benoit, R., Erre, R.: Spatial distribution of iron and sulphur species on the surface of pyrite. Appl. Surf. Sci. **68**, 81–93 (1993)
49. Descostes, M., Mercier, F., Thromat, N., Beaucaire, C., Gautier-Soyer, M.: Use of XPS in the determination of chemical environment and oxidation state of iron and sulfur samples: constitution of a data basis in binding energies for Fe and S reference compounds and applications to the evidence of surface species of an oxidized pyrite in a carbonate medium. Appl. Surf. Sci. **165**, 288–302 (2000)
50. Zerulla, D., Chasse, T.: X-ray induced damage of self-assembled alkanethiols on gold and indium phosphide. Langmuir **15**, 5285–5294 (1999)
51. Heister, K., Zharnikov, M., Grunze, M., Johansson, L.S.O., Ulman, A.: Characterization of X-ray induced damage in alkanethiolate monolayers by high-resolution photoelectron spectroscopy. Langmuir **17**, 8–11 (2001)
52. Beamson, G., Briggs, D.: High Resolution XPS of Organic Polymers. John Wiley & Sons Ltd, Chichester, UK (1992)
53. Moulder, J.F., Stickle, W.F., Sobol, P.E., Bomben, K.D.: Handbook of X-Ray Photoelectron Spectroscopy. Physical Electronics, Inc., Eden Prairie, MN, USA (1995)
54. McCafferty, E., Wightman, J.P.: Determination of the concentration of surface hydroxyl groups on metal oxide films by a quantitative XPS method. Surf. Interface Anal. **26**, 549–564 (1998)
55. Huang, N.P., Michel, R., Voros, J., Textor, M., Hofer, R., Rossi, A., Elbert, D.L., Hubbell, J.A., Spencer, N.D.: Poly(L-lysine)-g-poly(ethylene glycol) layers on metal oxide surfaces: surface-analytical characterization and resistance to serum and fibrinogen adsorption. Langmuir **17**, 489–498 (2001)
56. Heuer, J.K., Stubbins, J.F.: An XPS characterization of FeCO3 films from CO2 corrosion. Corr. Sci. **41**, 1231–1243 (1999)
57. Brundle, C.R., Chuang, T.J., Wandelt, K.: Core and valence level photoemission studies of iron-oxide surfaces and oxidation of iron. Surf. Sci. **68**, 459–468 (1977)
58. Olla, M., Navarra, G., Elsener, B., Rossi, A.: Nondestructive in-depth composition profile of oxy-hydroxide nanolayers on iron surfaces from ARXPS measurement. Surf. Interface Anal. **38**, 964–974 (2006)
59. Pinna, R.: Synthesis and characterization of Zn and Fe polyphosphates glasses. Diploma Thesis, University of Cagliari, Cagliari, Italy (2001/2002)
60. Onyiriuka, E.C.: Zinc phosphate-glass surfaces studied by XPS. J. Non-Cryst. Solids **163**, 268–273 (1993)
61. Brückner, R., Chun, H.-U., Goretzki, H., Sammet, M.: XPS measurements and structural aspects of silicate and phosphate glasses. J. Non-Cryst. Solids **42**, 49–60 (1980)
62. Brow, R.K., Arens, C.M., Yu, X., Day, E.: An XPS study of iron phosphate-glasses. Phys. Chem. Glass. **35**, 132–136 (1994)
63. Cumpson, P.J.: Angle-resolved X-ray photoelectron spectroscopy. In: Briggs, D., Grant, J.T. (eds.) Surface Analysis by Auger and X-Ray Photoelectron Spectroscopy, pp. 651–675. IM Publications and Surface Spectra Limited, Chichester and Manchester, UK (2003)
64. Piras, F.M., Rossi, A., Spencer, N.D.: Combined in situ (ATR FT-IR) and ex situ (XPS) study of the ZnDTP-iron surface interaction. Tribol. Lett. **15**, 181–191 (2003)
65. Minfray, C., Martin, J.M., Esnouf, C., Le Mogne, T., Kersting, R., Hagenhoff, B.: Antiwear mechanisms of zinc dithiophosphate: a chemical hardness approach. Thin Solid Films **447**, 272–277 (2004)
66. Stachowiak, G.W., Batchelor, A.W.: Engineering Tribology. Elsevier Inc., Oxford, UK (2005)
67. Bovington, C.H., Dacre, B.: The adsorption and reaction of decomposition products of zinc di-isopropyldiophosphate on steel. ASLE Trans. **27**, 252–258 (1984)
68. De Barros, M.I., Bouchet, J., Raoult, I., Le Mogne, T., Martin, J.M., Kasrai, M., Yamada, Y.: Friction reduction by metal sulfides in boundary lubrication studied by XPS and XANES analyses. Wear **254**, 863–870 (2003)
69. Pawlak, Z., Yarlagadda, P.K.D.V., Frost, R., Hargreaves, D.: The mechanical strength of phosphates under friction-induced cross-linking. J. Achieve. Mater. Manuf. Eng. **17**, 201–204 (2006)
70. Martin, J.M.: Antiwear mechanisms of zinc dithiophosphate: a chemical hardness approach. Tribol. Lett. **6**, 1–8 (1999)